Supporting Information for "An analytic model for Tropical Cyclone outer winds"

Timothy W. Cronin[1]

[1]Program in Atmospheres, Ocean, and Climate, MIT, Cambridge, Massachusetts, USA

Contents of this file

1. Text S1 to S5
2. Figure S1

Text S1: Fast calculation of multiple $G(r)$ profiles.

Matrix multiplication enables fast simultaneous calculation of $G(r)$ at many radial points and values of γ. The denominator y in $G(r)$ can be written as:

$$y = \sum_n \sum_l c_{n,l} \gamma^l [x^n/(n!)^2], \tag{1}$$

where the set of $c_{n,l}$ define a coefficient matrix C that depends on neither γ nor $x = 1 - r/r_0$. The coefficient of $[x^n/(n!)^2]$, or $(n!)^2 a_n = \sum_{l=0}^{\infty} c_{n,l}\gamma^l$, is a degree-$n$ polynomial in γ, defined by a linear, homogeneous, second-order recurrence relation with non-constant coefficients (Equation 10 in the main text, and note thereafter). I have found no closed-form solution for this recurrence, but an $N \times N$ coefficient matrix C needs only be computed once in

order to make many calculations of G. For example, a single value of y can be written as a product of a row vector of powers of x, the coefficient matrix C, and a column vector of powers of γ, with an expression for the first four terms in y as follows:

$$y = \underbrace{\left[\begin{array}{ccccc} x^0 & x^1 & \frac{x^2}{(2!)^2} & \frac{x^3}{(3!)^2} & \frac{x^4}{(4!)^2} \end{array}\right]}_{X} \underbrace{\left[\begin{array}{ccccc} 1 & 0 & 0 & 0 & 0 \\ 0 & 1 & 0 & 0 & 0 \\ 0 & 0 & 1 & 0 & 0 \\ 0 & 0 & -1 & 1 & 0 \\ 0 & 0 & -6 & -4 & 1 \end{array}\right]}_{C} \underbrace{\left[\begin{array}{c} \gamma^0 \\ \gamma^1 \\ \gamma^2 \\ \gamma^3 \\ \gamma^4 \end{array}\right]}_{\Gamma}. \tag{2}$$

To make many calculations at once, the row vector of powers of $x^n/(n!)^2$ is extended into a $K \times N$ (row $\times$ column) matrix X for K values of $x = 1 - r/r_0$, and the column vector of powers of γ is extended into a $N \times L$ matrix Γ for L values of γ. A $K \times L$ array of values of $y = XC\Gamma$ is thus given by matrix multiplication. The coefficients in $y'_{(x)}/\gamma$ can be written similarly, with a coefficient matrix C' obtained by deleting the first row and column of C, and multiplying the (new) n^{th} row by $n + 1$. The value of $G(r)$ is then calculated simultaneously for K points in radius and L values of γ using elementwise division of the matrices $y'_{(x)}/\gamma$ and y. Note that the factors $1/(n!)^2$ can be included in either powers of x or in the n^{th} row of C – they are written here in the matrix X, but numerical calculations (Cronin, 2023) include them in the matrix C for reasons of numerical precision ($(n!)^2$ becomes quite large).

Text S2: Approximations and convergence of $G(r)$.

I have not found any simplifications of $G(r)$ that are mathematically justified over the full range of r, but $G(r)$ can be approximated exactly near $r = r_0$ ($x << 1$) by a ratio of Bessel functions (dashed lines in Figure 2a). This approximation $G_b(r)$ is obtained by taking $1 - x \approx 1$ and $2 - x \approx 2$ in Equation 10 of the main text, which leads to an equation

for an approximate solution y_b:

$$x{y_{b(x)}}'' + {y_{b(x)}}' - \gamma y_b = 0. \tag{3}$$

Relevant solutions of this equation are $y_b = I_0\left[2\sqrt{\gamma x}\right]$, where I_0 is the modified Bessel function of the first kind of order 0; leading to approximate solution $G_b(r)$:

$$G_b(r) = \frac{1}{\sqrt{\gamma x}} \frac{I_1\left[2\sqrt{\gamma x}\right]}{I_0\left[2\sqrt{\gamma x}\right]}. \tag{4}$$

This approximate solution also corresponds to the functional form of a simplified recurrence relation $a_n = \gamma a_{n-1}/n^2$, or (equivalently) setting all off-diagonal elements in the coefficient matrix C to zero. Some effort was devoted to using this Bessel function approximation as an initial guess at $G(r)$, and refining this guess with an analytically-determined correction function (which would take the form of a power series), but numerical evaluation of Equation 4 was found to be slower than simply evaluating the full solution $G = y'_{(x)}/(\gamma y)$ derived in the main text.

Empirically, I have found that the approximation:

$$G_e(r) = (1 + \gamma x)^{-1/2 - x/6} \tag{5}$$

works rather well (dotted lines in Figure 2a). Maximum relative errors for G_e are small when γ is small, but grow with increasing γ to $\sim 15\%$ for $\gamma = 100$ and $\sim 35\%$ for $\gamma = 1000$. The form $[1 + \gamma x]^{-1/2}$ was chosen to match the limiting value and slope of G at $r = r_0$, and the addition of the term $-x/6$ to the exponent was purely empirical; there is no theoretical basis for this choice.

Another approximation merits brief mention: Emanuel (2004) suggests that the dominant balance of terms in Equation 4 of the main text is such that both sides approximately

equal zero, so that:

$$V(r) = \left(w_r f \frac{(r_0^2 - r^2)}{2 c_D r} \right)^{1/2}. \tag{6}$$

This can be rewritten in terms of V_{AMC} and a relative wind speed factor G_{E04}, as:

$$V(r) = V_{AMC}(r) \underbrace{\left[\left(\frac{2}{\gamma} \frac{r/r_0}{1-(r/r_0)^2} \right)^{1/2} \right]}_{G_{\mathrm{E04}}(r)}. \tag{7}$$

This form appears to be a good approximation at intermediate radii when γ is large, but since the term in brackets approaches zero at $r = 0$ and blows up as $r \to r_0$, it fails at both large and small radii.

It is not obvious from the series solution (Equations 11 and 12 in main text) that the quotient $y'_{(x)}/(\gamma y)$ must be constrained to lie on $[0, 1]$. Calculations show rapid convergence for small γ, and slowest convergence for large γ (e.g., Figure 2b). The recurrence relation (Equation 11 of the main text) is consistent with this result: it indicates that coefficients in the series will increase in magnitude roughly until $n > \sqrt{\gamma}$, and decay roughly as 2^{-n} at $n >> \sqrt{\gamma}$, suggesting that the required number of terms for convergence should scale with $\sqrt{\gamma}$. Since the range of values of γ for realistic cyclones is relatively constrained, good accuracy can be obtained if a number of terms several times as large as the square root of the greatest value of γ experienced is used (Figure 2b or other similar calculations can guide such decisions).

Text S3: Situations with no outer-wind component

A first-order approximation to $G(r)$ can be used to derive a condition on the values of $\tilde{w_Q}$ and Ro for which there is no outer wind component to the merged profile. The merged profile will consist of an inner-wind only profile if the inner and outer wind profiles do

not intersect on $0 < r < r_0$ when r_0 is set equal to $r_i = r_m(4V_x/(fr_x) + 1)^{1/2}$, the radius where the inner wind profile goes to zero. For the math in this section, it is sufficiently accurate to assume $V_x \approx V_m$ and $r_x \approx r_m$, so that $r_i/r_m = (4\mathrm{Ro} + 1)^{1/2}$.

I begin by rewriting Equation 13 of the main text as:

$$V_{\mathrm{in}} = f\frac{r_i^2 - r^2}{2r} \times \frac{(r/r_m)^2}{1 + (r/r_m)^2}, \tag{8}$$

which is akin to Equation 8 of the main text, in that it expresses the winds as an angular-momentum-conserving value, multiplied by a function of radius that lies between 0 and 1 and increases monotonically with increasing r. Equating the inner and outer wind profiles when $r_0 = r_i$ to solve for radii r^* where the two profiles intersect requires that $G(r^*) = (r^*/r_m)^2/(1 + (r^*/r_m)^2)$ for the outer wind profile. There will thus be no physical merge radius possible if the outer wind profile has $G(r) > (r/r_m)^2/(1+(r/r_m)^2)$ for all $0 < r < r_i$. Since this limit only appears to occur (see the gray shaded area in Figure 3) when $\tilde{w_Q}$ is large and γ is small, I use a first-order approximation of $G(r) \approx 1 - \gamma(1 - r/r_0)/2$ in γ. Rearranging the equality $G(r^*) = (r^*/r_m)^2/(1+(r^*/r_m)^2)$ with this small-γ approximation for $G(r)$ gives:

$$\frac{2}{\gamma} = (1 + (r^*/r_m)^2)(1 - r^*/r_0), \tag{9}$$

which will lack a solution if the maximum value of the right-hand side on $0 < r^* < r_0$ is less than the value of the left-hand side. In the limit that Ro is reasonably large, $r_0 = r_i \approx 2r_m\mathrm{Ro}^{1/2}$, and the value of the right-hand side maximizes at approximately $16\mathrm{Ro}/27$ for $r^* \approx 2r_i/3 >> r_m$. In this limit, the left-hand side can also be approximated as $2/\gamma \approx 2w_r/(2r_m\mathrm{Ro}^{1/2}fc_D) = Ro^{1/2}\tilde{w_Q}$. Equating these expressions indicates that the left-hand side will be larger than the maximum value of the right for all $0 < r^* < r_0$ if $\tilde{w_Q}$

exceeds some critical value $\tilde{w_Q}^*$, where:

$$\tilde{w_Q}^* = \frac{16\mathrm{Ro}^{1/2}}{27}. \tag{10}$$

Thus, if $\tilde{w_Q} > \tilde{w_Q}^*$, this argument indicates no outer-wind component; this region lies to the right of the dark gray dotted line in Figure 3.

Text S4: Benchmarking for merged wind calculations

I include MATLAB code that performs fast calculations of the merged $V(r)$ profiles (Cronin, 2023). The code is faster than previous approaches for two main reasons. First, a lookup table approach is used to store r_0/r_m, r_a/r_m (and thus also γ) as functions of $\tilde{w_Q}$ and Ro – this is feasible because analytic solutions to the outer wind profile allow storing entire profiles across a broad range of parameter space with only a few saved variables. the code interpolates from generic input values of $0.01 < \tilde{w_Q} < 10$ and $1 < \mathrm{Ro} < 100$ to obtain r_0/r_m and r_a/r_m, which determine γ and the radial domain of each wind model. Second, the code is fast because it is vectorized: the matrix approach above (Text S1) allows calculation of many values of $G(r)$ at once. These two improvements increase the calculation speed for wind profiles by a factor of ~ 50 relative to the code of Chavas (2022) (Figure S1a). The codes are compared by selecting 100 random points from parameter space with $17 < V_m < 77$ m s^{-1}, $15 < r_m < 115$ km, $5 \times 10^{-5} < f < 1.25 \times 10^{-4}$, and $0.001 < w_r < 0.005$ m s^{-1}, and a constant value of $c_D = 0.0015$. The lookup/matrix method described above gets faster in a relative sense for more profiles computed at once, so long as there is sufficient memory.

In terms of accuracy, differences between the two codes in azimuthal winds are typically on the order of 0.1 m s^{-1} (Figure S1b). Further testing suggests this small difference in

winds between the two codes arises from a combination of factors, including the precision of wind merger of the two profiles in both codes, the method of tweaking of V_x and r_x in the inner wind profile to ensure that $\max(V)$ occurs at $r = r_m$ in both codes, the table lookup interpolation and power series truncation errors in my method, and numerical integration errors in the approach of Chavas (2022). My code seems to be converged more closely to a "true" solution than calculations with default parameters of Chavas (2022), and the approach here can also use decreased grid spacing without degrading accuracy. Overall, the code presented here (Cronin, 2023) may be useful for risk modeling or probabilistic forecasting applications where it is desirable to simulate the effects of a very large number of realizations of wind profiles.

Text S5: Overturning streamfunction of the inner wind model

The overturning circulation and integrated vertical mass transport of a Tropical cyclone is given (under the assumption of a balance between radial advection of angular momentum and frictional torque) by rearranging Equation 1 of the main text:

$$\psi = \frac{c_D r^2 V^2}{dM/dr}, \tag{11}$$

where the overturning streamfunction ψ thus has units of $\mathrm{m}^3\ \mathrm{s}^{-1}$ (mass and volume transports are used interchangeably here following Emanuel, 2004, which is not completely accurate but suffices for the purposes here). Because V and dV/dr are continuous at the merge radius r_a, merged wind profiles are also continuous in dM/dr and ψ. Although not discussed as rationale by Chavas, Lin, and Emanuel (2015), continuity of the streamfunction is a critical reason to enforce continuity of dV/dr at the merge point. The inner wind profile of Emanuel and Rotunno (2011), with $c_k/c_D = 1$, has wind profile given by

Equation 13 of the main text, which can be rewritten for the sake of the scaling argument here using the approximate equalities $V_x \approx V_m$, $r_x \approx r_m$, and $V_x/(fr_x) \approx \text{Ro}$. The inner wind model thus has streamfunction:

$$\psi_{\text{in}} = \frac{c_D V_m r_m^2}{16\text{Ro}^2\left(1+\frac{1}{2\text{Ro}}\right)}\left(\frac{r}{r_m}\right)^3\left[(4\text{Ro}+1)-\left(\frac{r}{r_m}\right)^2\right]^2. \tag{12}$$

This inner streamfunction can be shown to maximize at $r/r_m = \sqrt{\frac{3}{7}(4\text{Ro}+1)}$, which is typically a considerably greater radius than $r_a/r_m \sim 3$ shown by Figure 3 (this result is also implied by the shape of the inner streamfunction in Figure 1). The positive value of $d\psi/dr$ at the merge point for the parameter space occupied by real-world storms indicates that r_a is generally small enough that inner circulation still has strong ascent there. This is consistent with the statement by Chavas et al. (2015) that the merged profiles represent an "ascending inner region" patched to a "descending outer region." This point should not be seen as a foregone conclusion because the inner wind profile itself contains both an inner ascending region where $r/r_m < \sqrt{\frac{3}{7}(4\text{Ro}+1)}$, and an outer descending region where $r/r_m > \sqrt{\frac{3}{7}(4\text{Ro}+1)}$.

Evaluating $\psi_{\text{in}}(r_a)$ gives the net upward mass transport by the storm. In the limits – reasonable for real-world storms – that Ro$>>$ 1 and $r_a/r_m << \sqrt{4Ro+1}$, this mass transport is given by:

$$\psi_{\text{in}}(r_a) \approx c_D V_m r_m^2 \left(\frac{r_a}{r_m}\right)^3. \tag{13}$$

This result is used further in the main text to explain the interdependence of V_m, r_m, and r_0 for merged profiles, and generally indicates strong sensitivity of the upward mass transport of a cyclone to the radius of the ascending region r_a.

References

Chavas, D. R. (2022, Jun). *Code for tropical cyclone wind profile model of Chavas et al (2015, JAS).* Retrieved from `https://purr.purdue.edu/publications/4066/1` doi: 10.4231/CZ4P-D448

Chavas, D. R., Lin, N., & Emanuel, K. (2015). A model for the complete radial structure of the tropical cyclone wind field. Part I: Comparison with observed structure. *Journal of the Atmospheric Sciences*, *72*(9), 3647–3662.

Cronin, T. W. (2023, Mar). *Code for "An analytic model for Tropical cyclone outer winds".* Retrieved from `https://doi.org/10.5281/zenodo.7783251` doi: 10.5281/zenodo.7783251

Emanuel, K. (2004). Tropical cyclone energetics and structure. *Atmospheric turbulence and mesoscale meteorology*(8), 165–191.

Emanuel, K., & Rotunno, R. (2011, 2012/01/04). Self-stratification of tropical cyclone outflow. Part I: Implications for storm structure. *Journal of the Atmospheric Sciences*, *68*(10), 2236–2249.

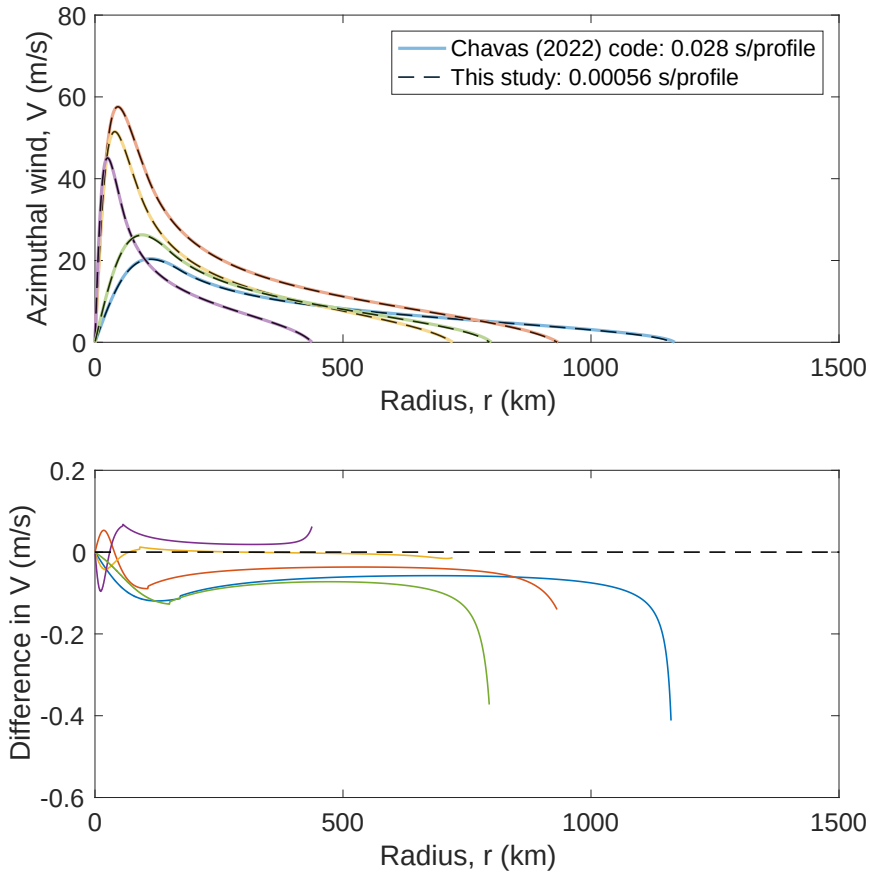

Figure S1. a) A set of five random wind profiles from a benchmark calculation on 100 random parameter values comparing the code from this study to the previous numerical method of Chavas (2022). b) Wind difference as a function of radius relative to the previous numerical method of Chavas (2022).